Lawrence Berkeley Laboratory
UNIVERSITY OF CALIFORNIA

Materials & Molecular Research Division

Submitted to Physical Review B

HIGH RESOLUTION ANGLE-RESOLVED PHOTOEMISSION STUDIES OF THE $\bar{M}$-POINT SURFACE STATE ON Cu(001)

S. D. Kevan and D. A. Shirley

December 1979

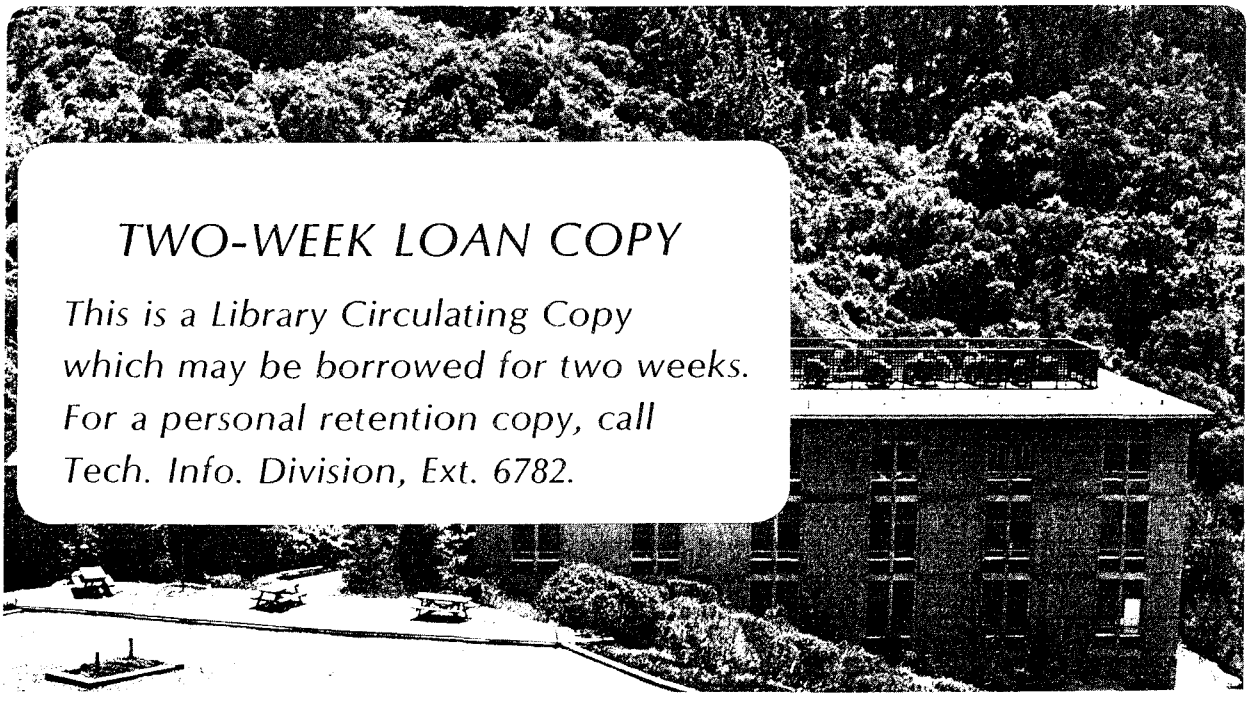

Prepared for the U.S. Department of Energy under Contract W-7405-ENG-48

LBL-10025

HIGH RESOLUTION ANGLE-RESOLVED PHOTOEMISSION STUDIES OF THE $\bar{M}$-POINT SURFACE STATE ON Cu(001)*

S.D. Kevan and D.A. Shirley

Materials and Molecular Research Division
Lawrence Berkeley Laboratory
and
Department of Chemistry
University of California
Berkeley, California 94720

December 1979

Abstract

High resolution angle-resolved photoemission studies were carried out on the surface state reported by Heimann et al. at the $\bar{M}$ point of the two-dimensional Surface Brillouin Zone of Cu(001). The symmetry of the state is shown to be odd with respect to the (100) mirror plane, as hypothesized by Heimann et al. Experimental $E(\vec{k}_{\parallel})$ dispersion relations in good agreement with the earlier study are reported, and accurate determinations of peak width as a function of $k_{\parallel}$ are shown to be reasonably well-fitted by a simple model. A novel temperature effect is reported along with a possible explanation.

---

*This work was supported by the Division of Chemical Sciences, Office of Basic Energy Sciences, U.S. Department of Energy under Contract No. W-7405-Eng-48.

I. Introduction

The application of high energy- and angular-resolution ($\leq$100 meV, $\leq 2^\circ$) in angle-resolved photoemission (ARP) studies of clean single-crystal surfaces has recently been shown to provide substantial increases in spectral information.[1-4] In a recent high-resolution experimental study, Heimann et al.[1] reported a surface state that had been predicted[5] at the $\bar{M}$ point in the two-dimensional Surface Brillouin Zone of Cu(001). Because this state lies at an energy slightly above the top of the bulk d-bands, the final-state hole lifetime is relatively long, and a very sharp peak is observed in the angle-resolved energy distribution curve (AREDC). High energy resolution was essential for an accurate description of the surface state.

Such a sharp peak is unusual in solid-state angle-resolved photoemission (ARP), and its existence suggested several interesting lines of investigation that we report in this paper. With sufficiently high angular and energy resolution, very accurate two-dimensional surface-state dispersion relations may be determined and, of equal interest, data on the evolution of the peak width with angle (and hence of the final-state lifetime with energy) are accessible. The utilization of polarized light permits the determination of surface-state symmetry, which in turn yields the orbital character. Finally, studies of the surface state temperature sensitivity give further information about surface-state character.

The organization of this paper is as follows: Section II describes our apparatus in more detail than we have given in the past. Section III describes experiments performed to characterize surface-state symmetry,

dispersion, and peak width. Section IV is concerned with a novel temperature effect, and the final section summarizes our results.

II. Experimental

The spectrometer used in these studies was designed to provide rapid data acquisition while allowing complete flexibility in orienting the vectors that are important in an ARP experiment. These vectors include the photon vector potential $\vec{A}$, the momentum vector of the photoelectrons that are detected, $\vec{p}$, the surface normal $\vec{n}$, and one or more directions that are required to describe the sample orientation relative to $\vec{A}$, $\vec{p}$, and $\vec{n}$ (e.g., crystalline axis directions). Because this is the first experiment in which we have systematically used these capabilities of the spectrometer, we have chosen to describe them in some detail here.

The heart of the spectrometer is a 5.4 cm mean radius 180° hemispherical sector energy analyzer. Before entering this analyzer, photoelectrons must pass through a lens composed of two Einzel lenses working in conjunction to focus electrons of a certain kinetic energy onto the entrance slit of the hemispherical analyzer at a fixed pass energy. Inside the lens are two collimators. The first, which lies between the Einzel lenses, will allow only those electrons emanating from the sample into a cone of half-angle $\sim 3°$ to be transmitted to the second lens, while the second collimator ensures that the maximum half-angle of electrons entering the analyzer is 2°. The actual half-angle collected off the sample can be determined by either collimator, depending on the kinetic energy-pass energy combination in conjunction with the Helmholtz-Lagrange law.[6] It turns out that for low pass energy and hence better energy

resolution, the second aperture limits the half-angle of electrons collected from the sample. This is the case for the present study, in which electrons in a cone of maximum angular dimensions of $1^\circ \times 2^\circ$ were collected. In some cases, rotations by $\frac{1}{2}^\circ$ produced significant spectral changes.

The analyzer is surrounded by two nearly continuous layers of μ-metal to reduce stray magnetic fields. In addition, a shield including one layer of silicon-iron and another of μ-metal have been constructed to fit about the periphery of the chamber. This shield reduces the field inside the chamber to <100 mG.

A schematic of the resistive anode multichannel detector system at the exit end of the analyzer is shown in Figure 1. A similar system has been described elsewhere.[7] Energy-analyzed electrons exit from the analyzer and are accelerated into an image-quality channel plate electron multiplier. The charge exiting from the channel plate is accelerated to a ceramic disk that has a uniform-thickness square of graphite evaporated on either side. On the front side, two contacts are made to opposite sides of the graphite layer along the "energy" (radial) direction, while on the back side contacts are made 90° away, concentric to the hemispheres. The charge (front side) and image charge (back side) resulting from a pulse are divided by the graphite resistances, collected at either set of contacts, amplified, and compared, yielding position sensitivity in two dimensions. The advantage of such a system is that a range of kinetic energies may be simultaneously analyzed using only four wires, thus allowing for the analyzer rotations described below. An enhancement of 20-30 in counting rate is obtained over a single-channel system. The amplification digit-

ization process requires 8-9 μsec, allowing maximum photoemission counting rates of 10^4/sec. This number will soon be tripled by electronic improvements.

The analyzer mount allows two-circle rotation through over 2π steradians of solid angle. This capability, combined with two axes of rotation on the sample manipulator and the capability of rotating the plane of polarization of a laboratory photon source, allows us to choose nearly any meaningful combination of directions of the vectors $\vec{A}$, $\vec{p}$, $\vec{n}$, etc.

The photon source used in these studies is a noble gas resonance lamp designed by N. J. Shevchik.[8] We have added a three-reflection polarizer that allows the plane of polarization to be rotated continuously through 180°. The calculated polarizations at the NeI and HeI resonance energies (16.83 eV and 21.22 eV) of 99^+% appear to be nearly realized, as is the calculated transmission of 10%. Some photoemission spectra at the HeII energy (40.8 eV) have also been collected, but the intensity is quite low and the polarization appears to be only ∿70-80%.

The analyzer and lamp are mounted on an ultrahigh vacuum chamber equipped with standard sample preparation facilities. LEED and Auger electron spectroscopy are used to characterize the clean and adsorbate covered surfaces. Facilities for beam dosing, cleaving, sputtering, and residual gas analysis are also included.

For the present studies, a single crystal of copper was oriented and cut to within 1° of the (001) face and etched in a solution of sodium 2-mercaptobenzimidazole-5-sulfonate and polyethylene glycol 400 in HCl to remove the surface damage layer.[9] The spectrometer was baked at 200°C to yield a base pressure of 2×10^{-10} Torr. The crystal was cleaned

in situ by repeated cycles of argon ion sputtering followed by annealing at 600° C. No surface impurities were detected by AES, and a sharp LEED pattern, indicative of an ordered (1×1) surface, was obtained. The surface was stable and remained clean for several hours. All angles were measured by laser autocollimation, and were reproducible to ±0.5°.

III. Surface-State Dispersion and Linewidth

As noted above, the sharpness of the surface state at the $\bar{M}$ point on Cu(001) permits several interesting experiments. The apparatus described in Section II provides slightly better angular and probably also better energy resolution than that used in the previous study.[1] The addition of polarized light also allows us to both confirm and extend the earlier work.

Let us begin with the determination of surface state symmetry. In Figure 2 we show AREDCs collected with identical experimental geometries, except that in the upper curve the light is s-polarized ($\vec{A}$ is odd with respect to the (100) mirror plane), while the lower curve is p-polarized ($\vec{A}$ is even). The peaks labeled A, B, and C are identified with those seen by Heimann et al.[1] and are labeled similarly. Peak A is identified as arising from the surface state of interest. At the emission angle in Figure 1, corresponding to emission from the $\bar{M}$ point, the peak is seen to be quite sharp. Using symmetry arguments, the surface state and peak B are clearly odd with respect to the mirror plane, while peak C is even.[10] The surface state was predicted to be mainly of d character.[5] In an atomic sense, it must be composed of d_{xy} and/or d_{yz} orbitals if the z-axis is chosen as the surface normal. Heimann et al.[1] argued that the state

should have atomic orbital symmetry d_{xy}, and our results clearly support their arguments. Since the surface state is derived from the highest occupied bulk band in the projected three-dimensional density of states, it is reasonable to expect that peaks A and B should be of the same symmetry.

Heimann et al.[1] also determined the two-dimensional dispersion relation of the surface state. We have done so as well. Our results, shown in Fig. 3 for initial states with $k_{\parallel}$ along $\bar{\Gamma} \rightarrow \bar{M} \rightarrow \bar{\Gamma}$, are in fairly good agreement. Also shown in Figure 3 is a plot of experimental peak width, a quantity that has been receiving increasing attention in the literature recently.[4,11,12] Qualitatively, the curve shows the pleasing result that the peak is sharpest at $\bar{M}(k_{\parallel} = 1.74\ A^{-1})$, the top of the surface-state band. While the experimental peak width is a convolution of the inherent peak width and the analyzer resolution function, the curve supports the idea that we are measuring mostly natural line width, since there is no flatness at the bottom of the curve. Further evidence that we are measuring the natural width is shown in Figure 4, where expanded AREDCs are plotted with the same resolutions as in Figure 3 as well, and two and four times lower resolution for the initial state at $\bar{M}$. The peak clearly broadens, but the width is well-fitted by the convolution

$$\Gamma \approx \sqrt{(\Delta E_A)^2 + (\Delta E_L)^2}$$

where ΔE_L is the natural line width of $\sim$50 meV and ΔE_A is the analyzer resolution, set at 30, 60, and 120 meV for the three curves in Figure 4.

Heimann et al.[1] claimed that the natural width should be ∿6 meV, based on extrapolation of a straight line fit of analyzer pass energy versus peak width to zero pass energy. We argue here that such a procedure is not valid since their data should in fact be described by a convolution relationship similar to what we have used above. The amount of scatter they observed at the lower pass energies could well be attributed to this very effect, and their straight line extrapolation would then yield a value for the natural width which is much too low. We note that their narrowest observed line had a FWHM of 50-60 meV, in good agreement with our result. We also emphasize that their data and ours are in good agreement: extrapolating our data as they do would also yield a very narrow line, which we believe is erroneous.

Perhaps the strongest evidence that the natural width is measured in Figure 3 is obtained from the peak shape. If $\Delta E_A \leq \frac{1}{2} \Delta E_L$, then the observed width will be dominated by the natural width and the shape will be essentially Lorentzian. If, on the other hand, $\Delta E_L \leq \frac{1}{2} \Delta E_A$, the lineshape will mimic the analyzer resolution function, which is triangular. In Figure 5, we show the leading edge of the top curve in Figure 4 expanded and fitted to both a Lorentzian and a triangle.[13] The characteristic Lorentzian tail is clearly seen in our peak shape, while the triangle does not fit nearly as well. It must, of course, be realized that we still have finite angular resolution, which will lead to broadening in a non-standard way. Because the sharpest peak (55-60 meV) we have observed is almost the same as that reported by Heimann et al., in spite of the fact that our angular resolution is better, and because the peak width, though sensitive to angle, does not change appreciably by rotations of our

(noncircular) acceptance cone, we infer that angular broadening is not a problem. Hence, we conclude that the natural width is ∿50 meV, and that the curve in Figure 3 is meaningful.

The natural line width Γ plotted in Figure 3 will in general be a function of both the final-state hole and electron lifetimes. It is straightforward to show that

$$\Gamma = \frac{(\Gamma_h + \Gamma_e \, v_h/v_e)}{1 - v_h/v_e}$$

where Γ_h and Γ_e are the linewidths due to the final-state hole and electron lifetimes, respectively, and $v_h = |\nabla_k E_i(k)|$, $v_e = |\nabla_k E_f(k)|$ are the final-state hole and electron velocities.[4,11,12] As explained elsewhere,[4,11,12] the peak width formula becomes simple for flat initial-state bands:

$$\Gamma \approx \Gamma_h + (v_h/v_e)\Gamma_e \approx \Gamma_h \, .$$

Near the $\bar{M}$ point, the surface state band is flat and v_h is small so that, as a first approximation, we may neglect all but the first term and take $\Gamma \approx \Gamma_h$. Assuming further that the surface-state dispersion relation can be fitted by

$$E(\vec{k}_\parallel) = E_0 - \alpha k_\parallel^2 \, ,$$

a simple model for the peak width as a function of initial energy can be derived as follows: Assume that Γ_h, the final-state hole lifetime, is proportional to $1/N_>(E)$, where $N_>(E)$ is the number of filled electron states of energy greater than E, which are thus energetically available

to fill the hole via the Auger process:

$$N_{>}(E) = \int_{E}^{E_F} N(E)\, dE = N_0 + \int_{E}^{E_0} N(E)\, dE \ .$$

Here, N_0 is the constant contribution from the s-p "plateau" above E_0. The electronic density of states for the two-dimensional dispersion relation we have chosen is

$$N(E) = 1/2\pi\alpha \qquad E < E_0$$
$$= 0 \qquad E > E_0 \ .$$

We see that

$$N_{>}(E) = N_0 + (1/2\pi\alpha)(E - E_0)$$

and since $N_{>}(E)$ is expected to be proportional to the linewidth, we get

$$\Gamma(E) = \Gamma_0 + \beta(E - E_0)$$

where β is approximately a constant. A plot of $\Gamma(E)$ versus $E - E_0$ is shown in Figure 6. Aside from substantial scatter arising from the difficulty in determining $\Gamma(E)$ accurately, the points do lie on a straight line. We also show data taken on a line perpendicular, but equivalent to, the $\bar{\Gamma} \rightarrow \bar{M} \rightarrow \bar{\Gamma}$ line, as shown in the inset. This model is oversimplified, but clearly the ideas are applicable in some general sense. A similar linear effect was observed without explanation by Knapp et al.[12] We note that the first correction to be made to the model is the addition of the $(v_h/v_e)\Gamma_e$ term, which will provide a small correction that scales approximately as $(E - E_0)^{\frac{1}{2}}$ since Γ_e and v_e are expected to be essentially constant over the very narrow range of dispersion studied here. The

major assumptions of the model (independence of Γ_n from E, quadratic dispersion, etc.) become better when $E \approx E_0$, so that the limiting behavior should be linear. The consistency of this simple model again strongly indicates that we measure natural linewidths.

IV. Temperature Dependence

We now turn our attention to a novel temperature effect. Previous photoemission and LEED temperature-dependent phenomena have usually been explained in terms of a Debye-Waller factor.[14-16] This implies that intensities decrease exponentially with temperature, a functional form that is accurately obeyed in LEED studies[17] and reasonably well-obeyed in photoemission studies of bulk bands.[14] One might therefore expect to be able to determine a surface Debye temperature by measuring the temperature dependence of a surface-state intensity.

In Figure 7 we show a series of AREDCs collected with $k_{\parallel}$ at the $\bar{M}$ point, for various sample temperatures. The intensity of the surface state is quite sensitive to temperature, much more so in fact than are the bulk features. The surface state essentially vanishes by 450° C, whereas the bulk features have decreased in peak intensity by only 10%. The magnitude of the effect is much larger than observed on the Cu(111) surface state.[19] We note here that the effect is completely reversible as the temperature returns to room temperature, and that it was observed to be reproducible on three different runs. Care was taken to exclude systematic errors.

Of equal importance is the functional form of the decrease in surface-state intensity, shown in Figure 8. At lower temperatures, the

intensity decreases nearly linearly, while the negative slope increases at higher temperature. The decrease is certainly not exponential. This, combined with the magnitude of the effect compared to the smaller (10-20%) decrease seen in LEED studies[17] at these energies, indicates that the decrease does not follow a simple Debye-Waller factor. By contrast, LEED patterns taken as a function of temperature showed only a gradual decrease in spot contrast, while Auger spectra showed no contamination, even at higher temperatures. Variations in lattice constant are expected to be small ($\leqslant$2%) and should not cause any substantial effect.

One possible explanation of the effect is a temperature-induced destruction of the surface state. This is plausible because our higher temperatures were 2-3 times the Debye temperature of copper so that short wavelength phonon modes would be significantly populated. This is especially true at the surface, where the effective Debye temperature is lower than in the bulk. The argument is even more reasonable when one considers that this surface state is highly localized to the top layer of atoms. Vibrational amplitudes from these short wavelength phonons might be expected to produce substantial rehybridization at the surface, with the consequent destruction of the surface state. Put more simply, the state disappears when the surface loses its two-dimensionality. A similar explanation has been used in the case of noble metal halides.[18]

V. Summary

The purpose of this paper has been to present data relevant to both the characterization of the $\bar{M}$-point surface state on Cu(001) and

to the clarification of the photoemission process involved. We have shown that the surface state has odd symmetry with respect to the $\bar{\Gamma} \rightarrow \bar{M}$ mirror plane, as hypothesized in an earlier study. The dispersion relation measured previously has been confirmed. We have presented data that indicate the natural peak width of the state at the $\bar{M}$ point is $\sim$50 meV, and have traced the evolution of the surface-state peak width as it disperses toward the d-bands. A simple model was presented that provided qualitative agreement with the peak width data. Finally, a novel temperature effect was described and a possible explanation was given. Clearly, further studies of the temperature dependence of surface-state intensities are in order.

References

1. P. Heimann, J. Hermanson, H. Miosga, and H. Neddermeyer, Phys. Rev. Letters 42, 1782 (1979); and Phys. Rev. B20, 3059 (1979).

2. S.G. Louie, P. Thiry, R. Pinchaux, Y. Petroff, D. Chandesris, and J. Lecante, submitted to Phys. Rev. Letters.

3. P. Heimann, H. Miosga, and H. Neddermeyer, Phys. Rev. Letters 42, 801 (1979).

4. P. Thiry, D. Chandesris, J. Lecante, C. Guillot, R. Pinchaux, and Y. Petroff, Phys. Rev. Letters 43, 82 (1979).

5. J.G. Gay, J.R. Smith, and F.J. Arlinghaus, Phys. Rev. Letters 42, 332 (1979).

6. See, for example, C.E. Kuyatt, "Electron Optics Lectures," unpublished.

7. M. Lampton and C.W. Carlson, Rev. Sci. Instrum. 50, 1093 (1979).

8. N.J. Shevchik, to be published.

9. J.S. Ahearn, J.P. Monaghan, and J.W. Mitchell, Rev. Sci. Instrum. 41, 1853 (1970).

10. J. Hermanson, Sol. State Commun. 22, 9 (1977).

11. D.E. Eastman, J.A. Knapp, and F.J. Himpsel, Phys. Rev. Letters 41, 825 (1978).

12. J.A. Knapp, F.J. Himpsel, and D.E. Eastman, Phys. Rev. B19, 4592 (1979).

13. The triangle is broadened at its base due to the α^2 term in the analyzer resolution function. Since $\alpha^2 \sim (1/3)(w/2R_0)$ in our case, the broadening is small and is indicated in the figure (see Ref. 6).

14. R.S. Williams, P.S. Wehner, J. Stöhr, and D.A. Shirley, Phys. Rev. Letters 39, 302 (1977).

15. N.J. Shevchik, Phys. Rev. B16, 3428 (1977); N.J. Shevchik, J. Phys. C10, L555 (1977).

16. J.P. Pendrey, Low Energy Electron Diffraction, Chap. 6, Academic Press, 1974.

17. R.S. Bauer, S.F. Lin, and W.E. Spicer, Phys. Rev. B14, 4527 (1976).

18. J.A. Knapp, F.J. Himpsel, A.R. Williams, and D.E. Eastman, Phys. Rev. B19, 2844 (1979).

Figure Captions

Figure 1. Resistive anode detection system schematic.

Figure 2. High resolution AREDCs of Cu(001). Initial states at the $\bar{M}$ point of the two-dimensional Brillouin zone are sampled. Upper curve: polarization vector is in the surface plane, parallel to (010). Lower curve: polarization vector is in (100) mirror plane.

Figure 3. Experimental dispersion relations and peak widths for the surface state near the $\bar{M}$ point. $|k_{\parallel}| = 1.74$ Å for initial states at the $\bar{M}$ point.

Figure 4. AREDCs of Cu(001) for initial states at the $\bar{M}$ point taken with three different analyzer resolutions. Top curve: same resolution as Figs. 2 and 3. Middle and bottom curves: resolution 2 and 4 times poorer than top panel.

Figure 5. Leading edge of top curve in Fig. 4 expanded and fitted to a Lorentzian (solid curve) and a triangular (dashed curve) lineshape.

Figure 6. Variation of the surface-state peak width with initial energy.

Figure 7. High resolution AREDCs of Cu(001) for initial states at the $\bar{M}$-point at various temperatures. Geometry is the same as Fig. 2, upper curve. Note dramatic decrease in surface state intensity at high temperature.

Figure 8. Plot of surface state intensity (solid curve) and its logarithm (dashed curve) vs absolute intensity.

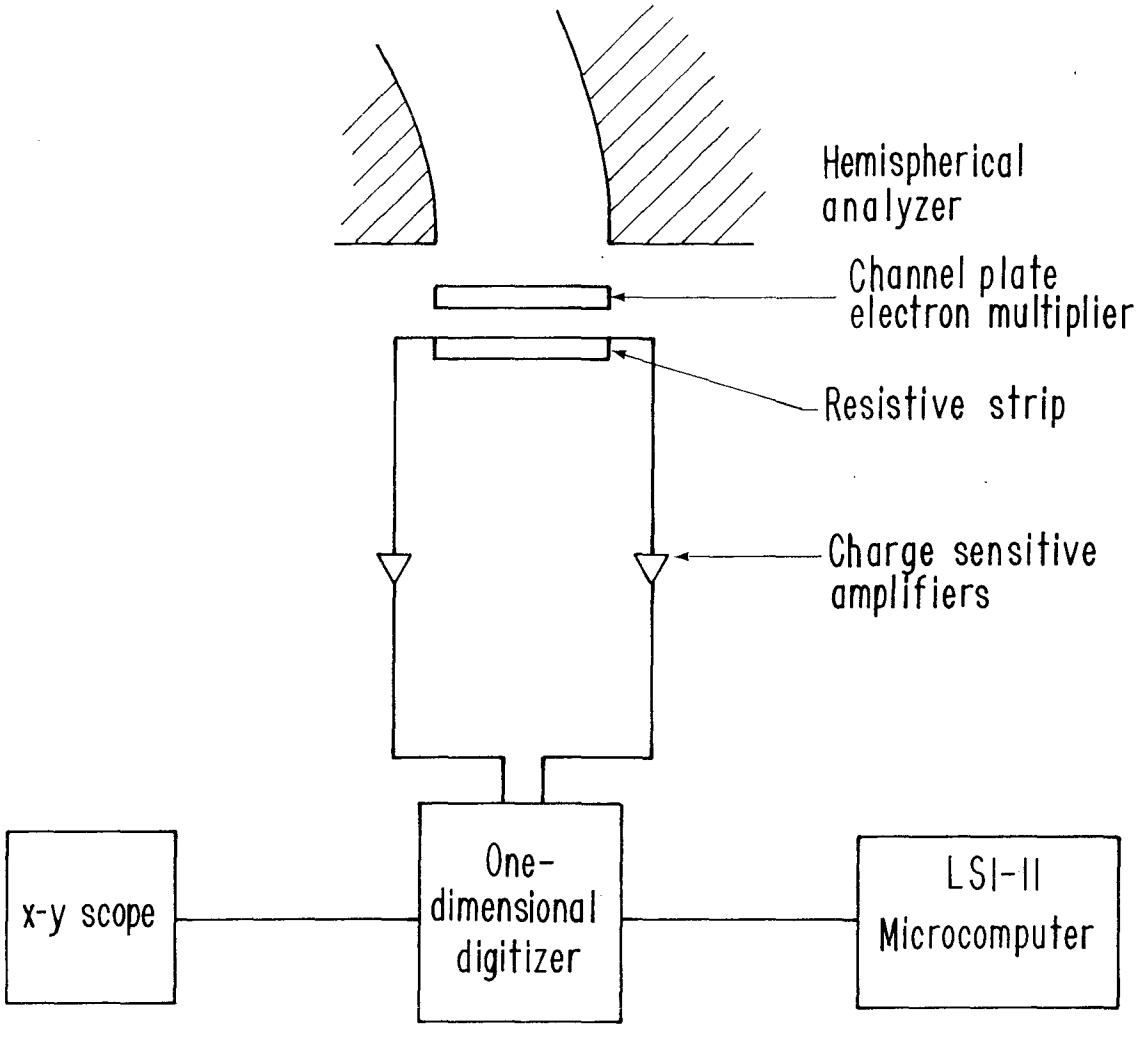

ARPES Detector electronics

XBL 7810-6548

Figure 1

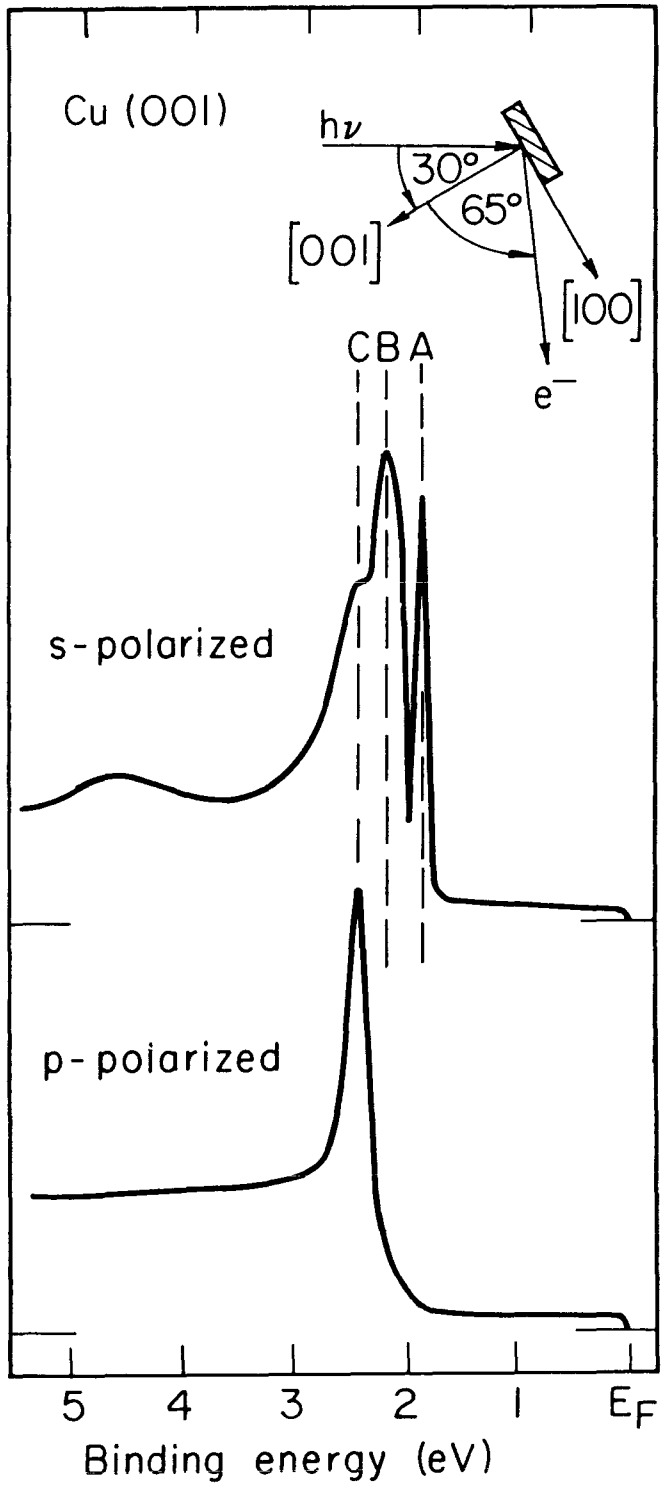

XBL7912-3932

Figure 2

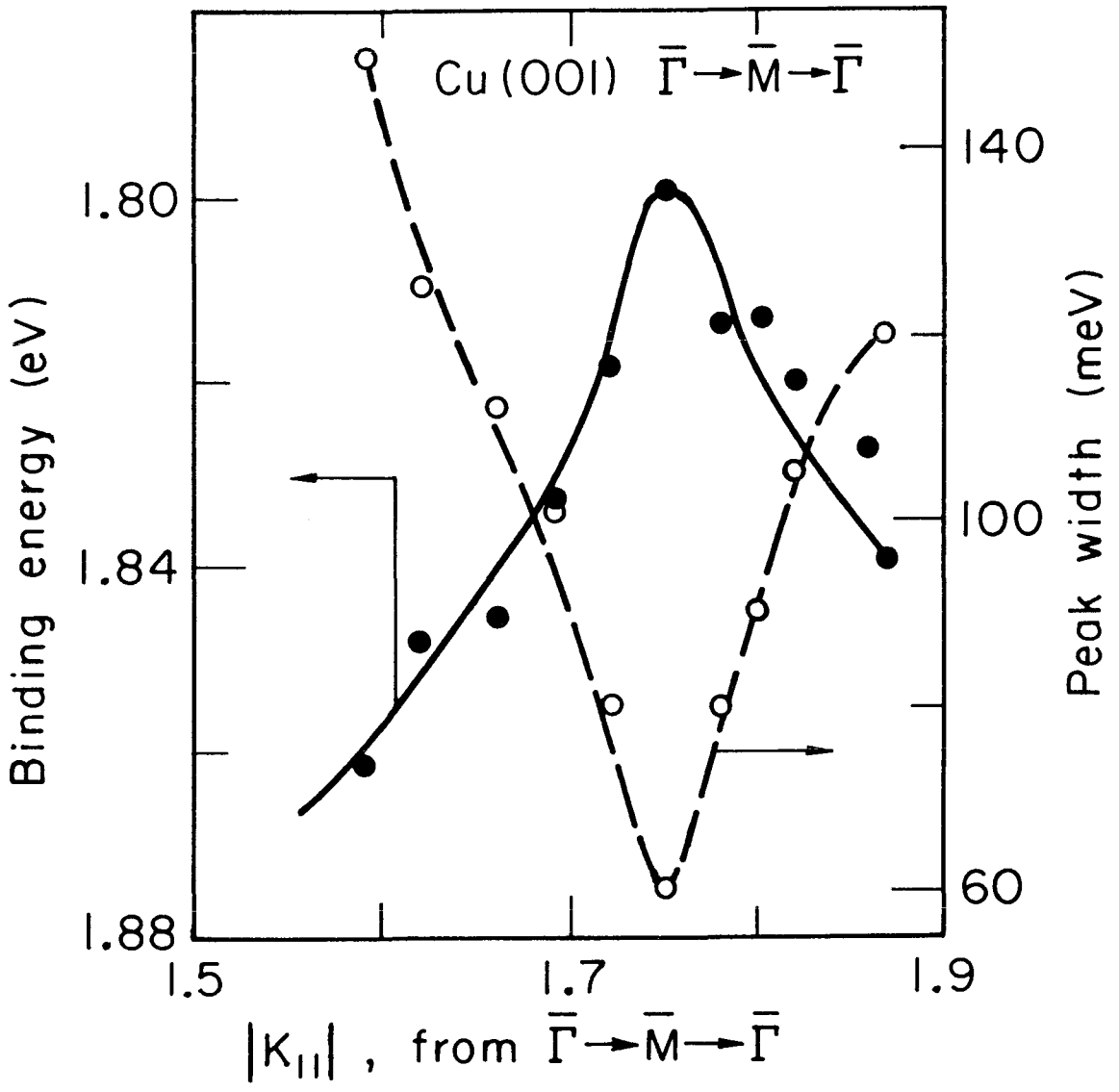
Cu(001) $\bar{\Gamma}\rightarrow\bar{M}\rightarrow\bar{\Gamma}$
Binding energy (eV)
1.80
1.84
1.88
Peak width (meV)
140
100
60
1.5
1.7
1.9
$|K_{\parallel}|$, from $\bar{\Gamma}\rightarrow\bar{M}\rightarrow\bar{\Gamma}$
XBL7912-3929

Figure 3

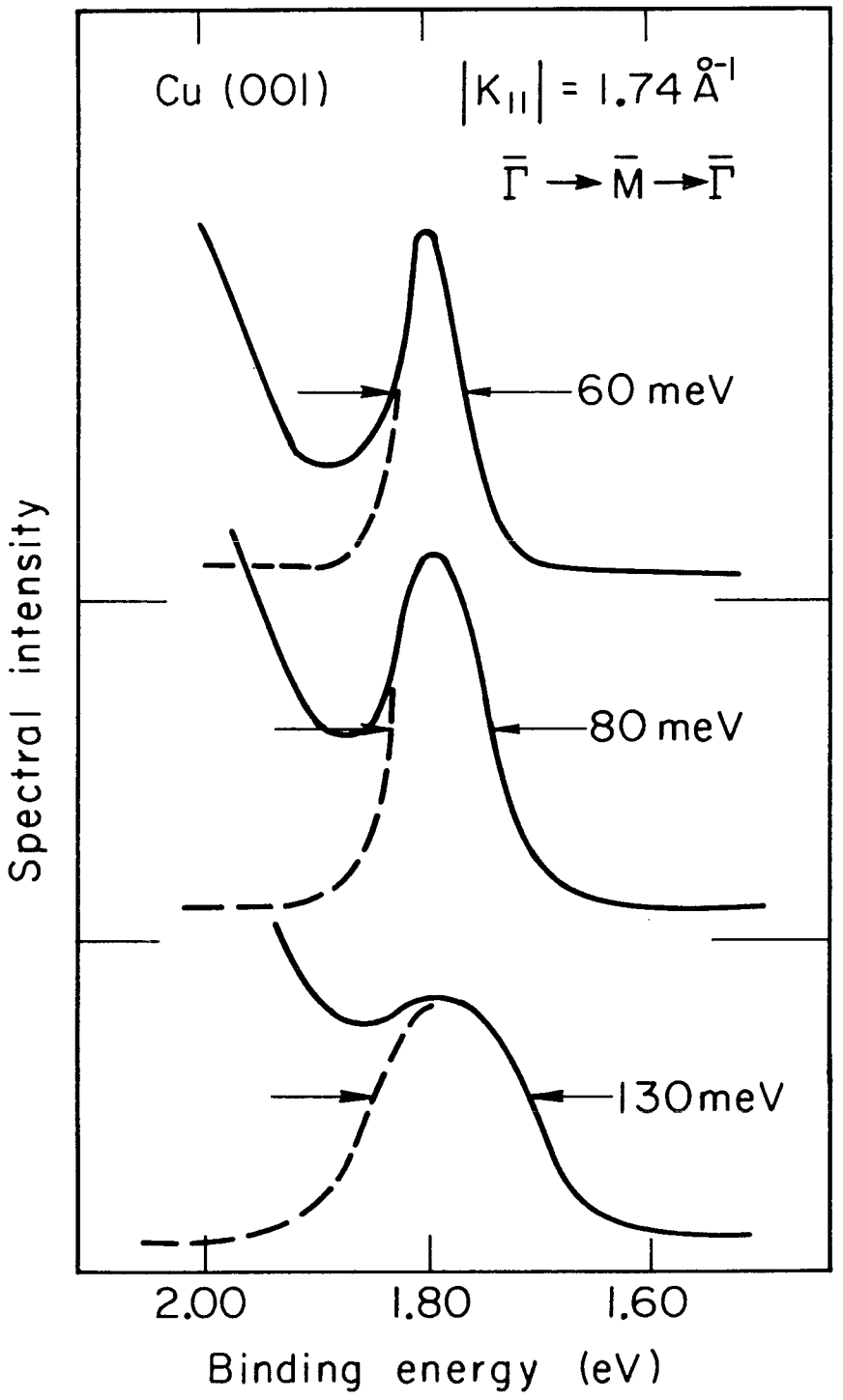

XBL7912-3930

Figure 4

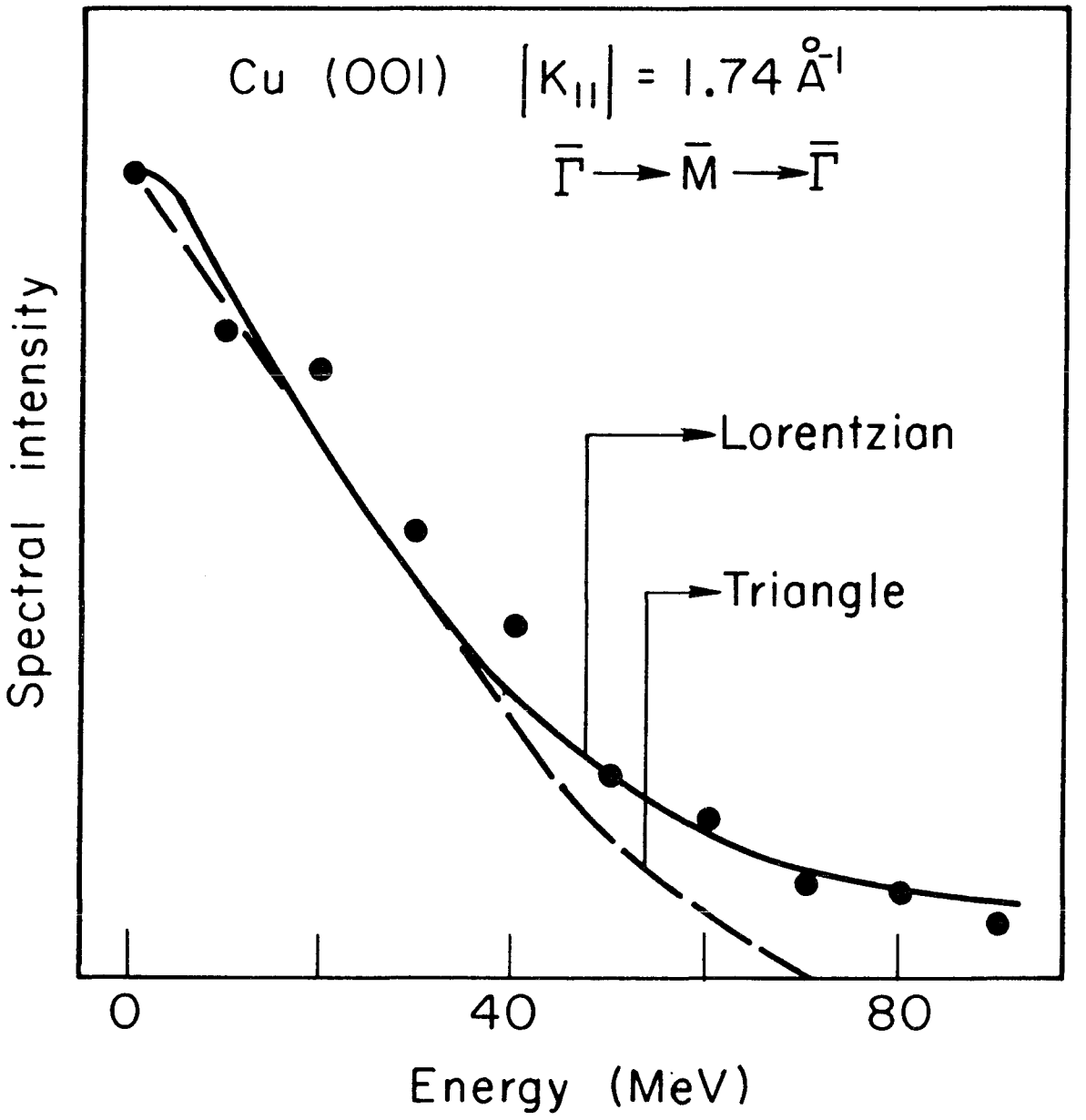

XBL7912-3927

Figure 5

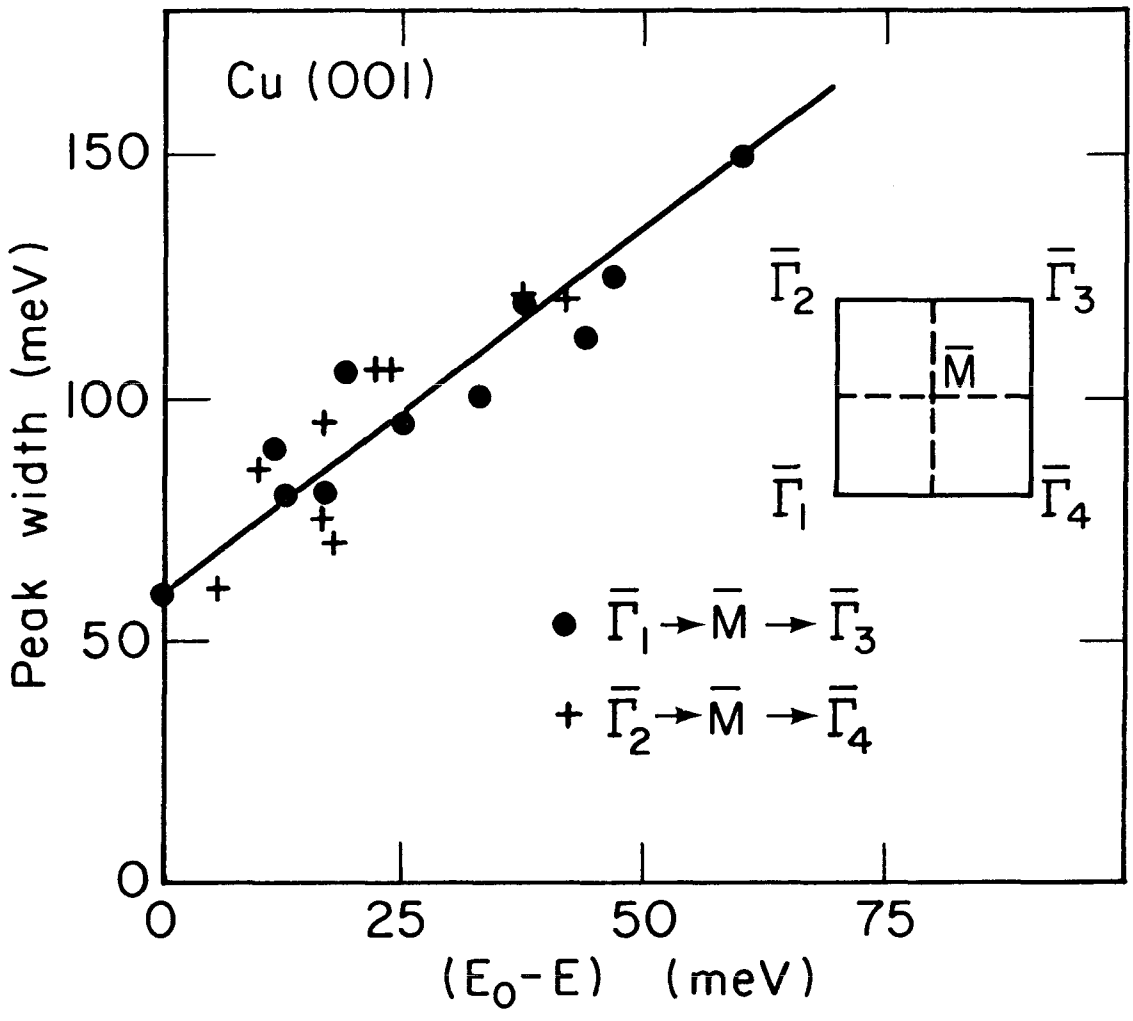

XBL7912-3928

Figure 6

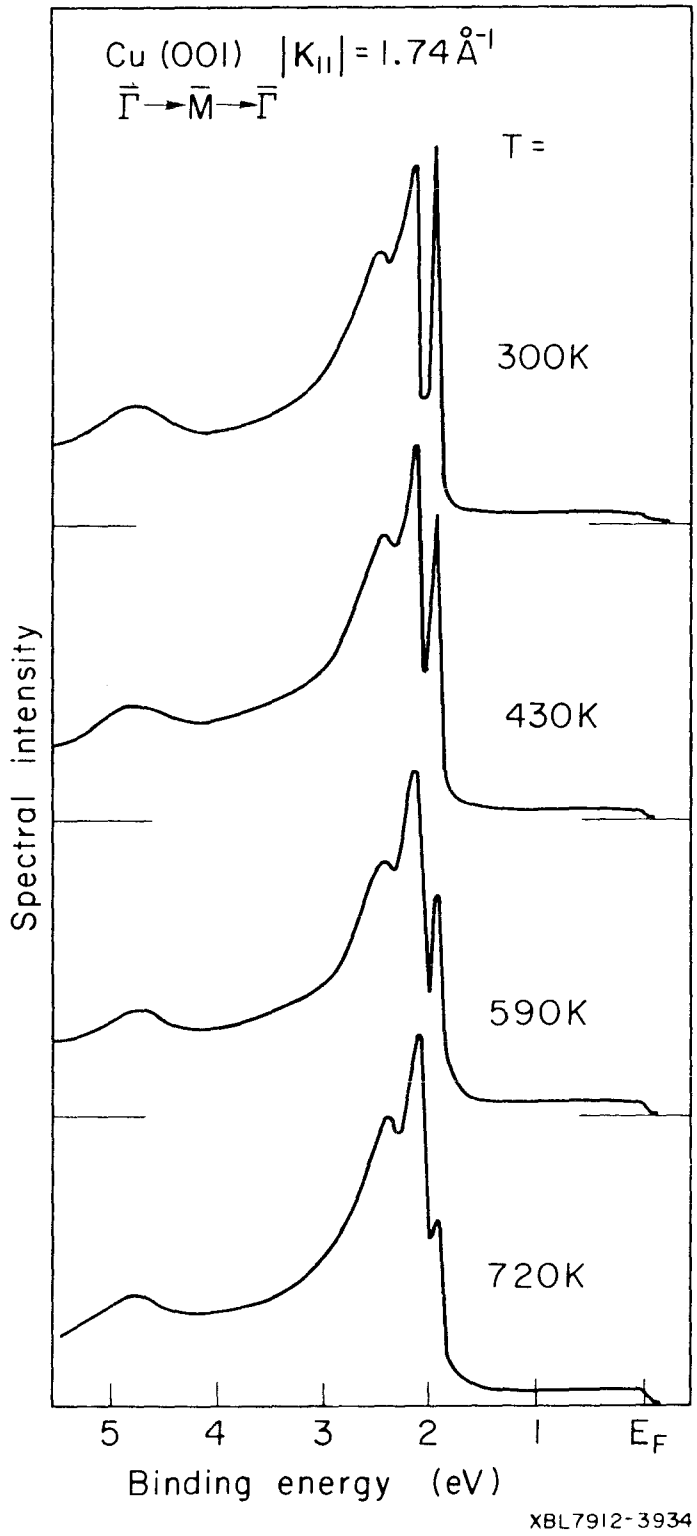
Cu (001) $|K_{\parallel}| = 1.74\,\text{Å}^{-1}$
$\bar{\Gamma} \rightarrow \bar{M} \rightarrow \bar{\Gamma}$
T =
300K
430K
590K
720K
Spectral intensity
5
4
3
2
1
E_F
Binding energy (eV)
XBL7912-3934

Figure 7

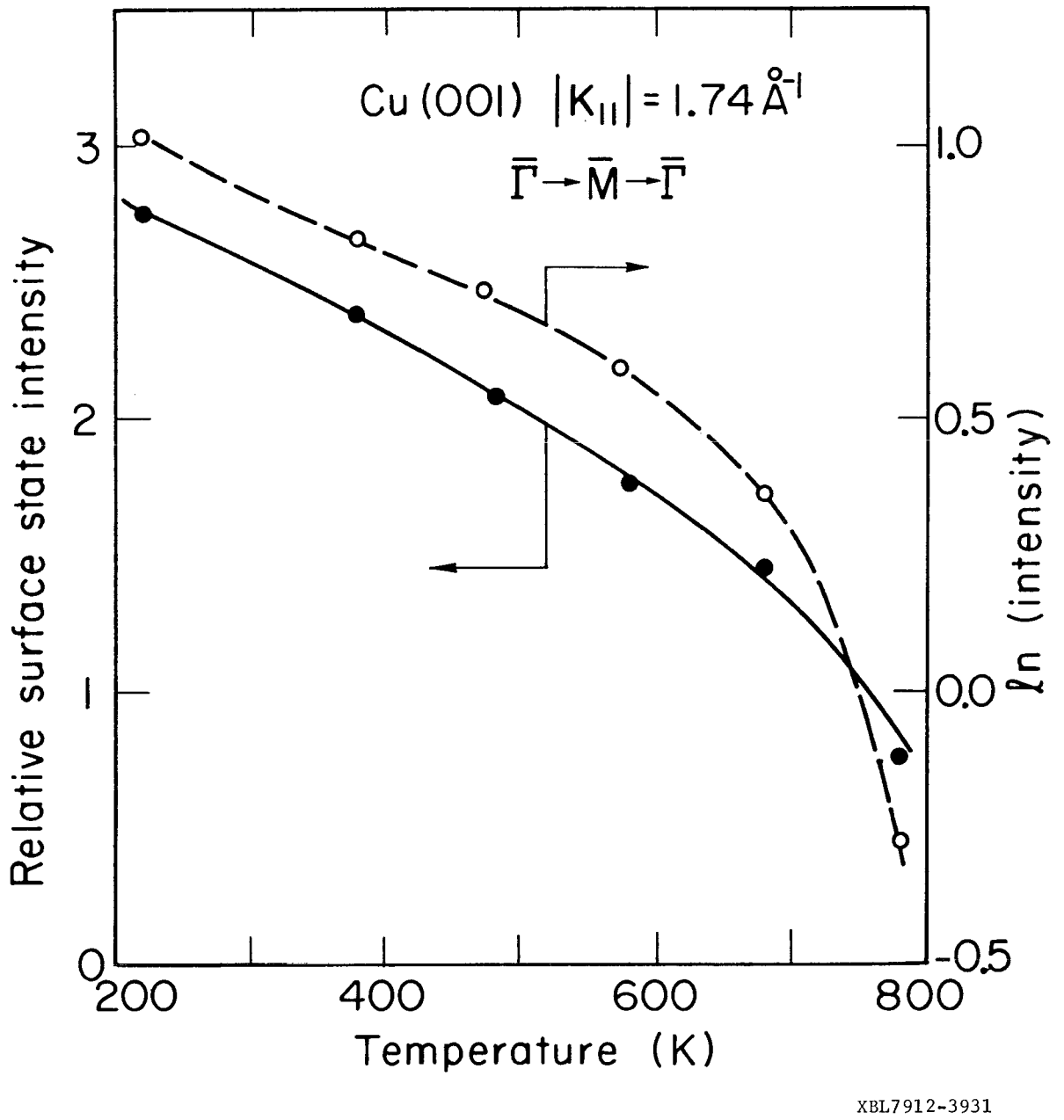
Cu (001) $|K_{\parallel}| = 1.74\ \text{Å}^{-1}$
$\bar{\Gamma} \rightarrow \bar{M} \rightarrow \bar{\Gamma}$
Relative surface state intensity
ln (intensity)
Temperature (K)
0
1
2
3
-0.5
0.0
0.5
1.0
200
400
600
800
XBL7912-3931

Figure 8